Mechanochemical Synthesis of Dispersible Platinum Nanosheets for Enhanced Catalysis in Microreactor

Koki Sasaki, Koji Miyake, Yoshiaki Uchida, and Norikazu Nishiyama*

Graduate School of Engineering Science, Osaka University, Toyonaka, Osaka 560-8531, Japan

ABSTRACT: Nanosheet fabrication usually requires some self-assembly process of the ingredients themselves or self-assembled templates to lead to the local anisotropy. Macroscopic forces and dynamics cannot usually generate the local anisotropy to synthesize nanosheets in a solution because the anisotropies of the macroscopic mechanical forces and dynamics are promptly relaxed in the molecular scale in a liquid phase. Here we report the mechanochemical synthesis of dispersible platinum nanosheets (PtNSs) using a microreactor. This work is the first example of bottom-up nanosheet synthesis of a non-exfoliable compound in a microflow reactor. The nanosheets grow through the lateral fusion of nanoplatelets in the hydrophilic space of the stable hyperswollen lyotropic lamellar (HL) phase of a surfactant solution. The lateral fusion is accelerated as the flow rate increases because the area of the bilayer in the HL phase increases with shear stress. Mechanical energy to promote the growth of the PtNSs can also be extracted in different ways. Most simply, syringe pumps electrically generate it. We also illustrate mechanochemical synthesis using gravity, the most universal and eco-friendly energy source on the earth. It is also the first example of the fabrication of anisotropic nanoparticles by using gravity. The larger PtNSs show higher catalytic activity for the reduction reaction from 4-nitrophenol to 4-

aminophenol due to their dispersibility; surprisingly, the exponential increase of the fusion patterns of nanoplatelets dramatically reduces the agglomeration of PtNSs. These PtNSs perform better in catalysis and should be promising for hydrogen production, fuel cells, and sensors because of their large surface area and dispersibility. This method could open up a pathway to valuable nanosheets.

KEYWORDS: Platinum nanosheets, Microreactor, Lamellar phase, Mechanochemical synthesis, Gravity.

INTRODUCTION

The properties of the nanostructured materials reflect their shape anisotropy.[1-4] The higher the aspect ratio of nanostructured noble metal is, the more its unique properties stand out: e.g., the catalytic activity of platinum nanosheets (PtNSs) and the near-infrared (NIR) absorption of gold nanotubes.[5,6] Nanostructured materials with shape anisotropy have been fabricated in various ways: seeding,[7] hydrothermal,[8] sol-gel,[9] soft-template[10] and hard-template[11] methods. In the fabrication of nanostructured materials, some self-assembly processes of the ingredients themselves or self-assembled templates are usually required to lead to the local anisotropy of the desired nanostructure by operating isotropic state functions like temperature and chemical composition, as shown in Figure 1a.[12-16]

Although pressure and flow rate are appropriate process variables for mass production and can be anisotropic, the global anisotropy cannot directly control the local anisotropy indispensable for the bottom-up synthesis of nanostructured materials in a solution.[17] It is because the macroscopic anisotropy is easily relaxed in the molecular scale in a simple liquid phase. Meanwhile, layered

solids can be mechanochemically exfoliated to give nanosheets (NSs) by shear stress, as shown in Figure 1b.[18] Local anisotropy intrinsic in the crystal structures converts the mechanical force to the anisotropic exfoliation. As similar anisotropic phases to the crystals, liquid crystalline (LC) phases with exceptionally long correlation time and length should be noticed in this context. Global anisotropic stimuli induce the change of the local anisotropy of the LC phases, such as molecular reorientation and pattern formation.[19,20] For example, shear stress also increases the order of the uniaxial symmetry of LC phases.[21]

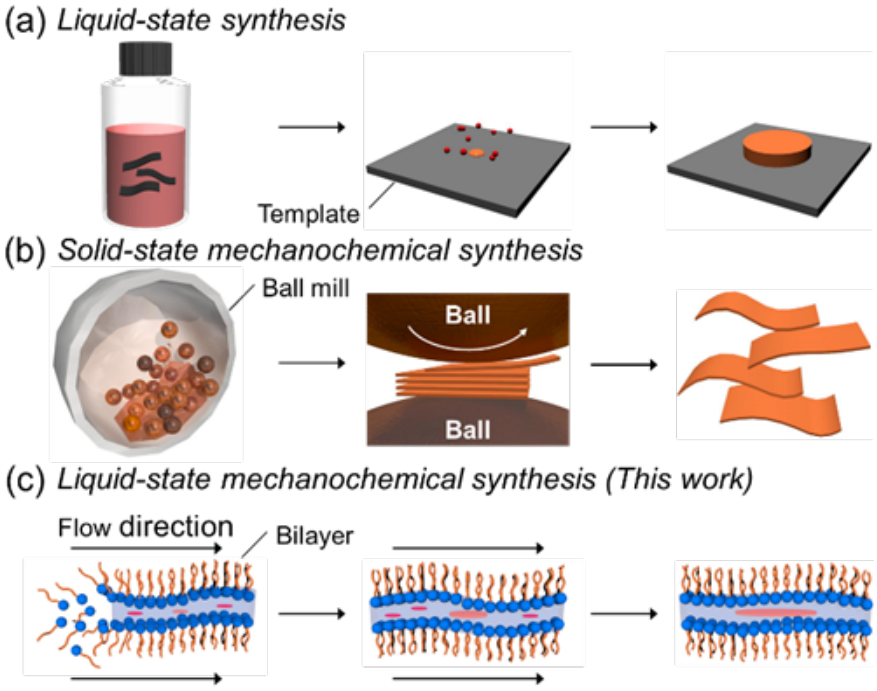

Figure 1. Schematic illustration of the synthesis method of NSs. (a) Conventional liquid-state synthesis used templates that promote anisotropic growth. (b) Solid-state mechanochemical synthesis exfoliates the layered materials by shear stress. (c) The present bottom-up method gives NSs due to the anisotropic fusion of nanoplatelets inside the two-dimensional reaction fields in an LC phase.

Both thermotropic and lyotropic LC phases have long correlation times and lengths.[22] The anisotropic growth can be controlled in a solution process using some LC phase as a solvent. 'Two-dimensional reactor in amphiphilic phases (TRAP) method' is one of the synthesis methods of NSs using hyperswollen lyotropic lamellar (HL) phases consisting of dispersed TRAPs,[23-27] bilayers with several nm thicknesses that keep several hundred nm intervals with each other.[28] The width of NSs synthesized using the TRAP method was reported to be proportional to the Reynolds number of the system determined by the size of the reaction vessel and agitator.[26] The NSs only grow in the in-plane direction through the lateral fusion of nanoplatelets, contributing to their dispersibility. Anisotropy and selectivity of reactions in the HL phases depend on the external macroscopic forces as when mechanochemical reactions occur in solid phases, as shown in Figure 1c.[29] It is consistent with the past literature reporting that the width of bilayers in the HL phase increases as the shear stress increases.[22] The shear stress as global anisotropy arising from the increasing flow rate of the reaction mixture should promote the growth of NSs.

We focused on the shape control of the nanostructured materials using a plug flow reactor; it should be regarded as a new kind of mechanochemical material synthesis, as shown in Figure 1c. The shear stress in the flow reactor with a uniform diameter depends only on the flow rate and viscosity of the reaction mixture. In particular, with a small change in the flow rate in microreactors, the particles' size and distribution have been reported to be precisely controlled over a wide range.[30,31] For NSs, the synthesis methods using microreactors are divided into top-down exfoliation[32] and bottom-up self-assembly.[33] None of them has used shear stress in microreactors to control the width of NSs yet. Here we report the mechanochemical synthesis of dispersible PtNSs in a TRAP solution using a microreactor to achieve higher dispersibility and catalytic activity together. This work is the first example of bottom-up nanosheet synthesis of a non-

exfoliable material in a microflow reactor. We also demonstrate the stable HL phases of the unprecedented mixture of a hydrophobic solvent and a non-ionic amphiphile appropriate as the TRAP solution for the hydrophilic PtNSs. This unprecedented HL phase would enable us to reuse the solvent and synthesize high-quality nanosheets in larger quantities and at lower costs. After showing that syringe pumps can electrically generate mechanical energy for the width expansion of PtNSs, we also illustrate mechanochemical control of the width using gravity, the most universal and eco-friendly energy source on the earth.[34] Pt has attracted attention due to its superior applications such as catalysis, hydrogen production, fuel cells, and sensors. To confirm that the PtNSs achieve the dispersibility and catalytic activity together, we discuss the dependence of a catalytic reaction from 4-nitrophenol to 4-aminophenol on the width of the PtNSs.[35]

MATERIALS AND METHODS

Materials. Heptane, methanol, ethanol, 1-propanol, 1-butanol, 1-pentanol, sodium hydroxide and hydrogen hexachloroplatinate (IV) hexahydrate ($H_2PtCl_6 \cdot 6H_2O$) were purchased from Wako Pure Chemical Industries Co. Sodium borohydride ($NaBH_4$) was purchased from Tokyo Chemical Industry Co., Ltd. Brij L4 was purchased from Merck KGaA. The water used was obtained from a water purifier (Direct-Q UV, Millipore Co.) with a resistivity of 18.2 MΩ cm.

Synthesis of platinum nanosheets by using a syringe pump. Platinum nanosheets (PtNSs) were synthesized through a microreactor in the hyperswollen lyotropic lamellar (HL) phases. The heptane solution (21 mL) with $H_2PtCl_6 \cdot 6H_2O$ (1.0×10^{-1} wt%), Brij L4 (6.9 wt%), water (1.9 wt%), and methanol (8.7×10^{-1} wt%) and the heptane solution (21 mL) with $NaBH_4$ (2.6×10^{-2} wt%), Brij L4 (6.9 wt%), sodium hydroxide solution (pH 11) (1.9 wt%), and methanol (8.7×10^{-1} wt%) were separately poured through PTFE tubing into a mixer. The mixture was pumped into a reaction

tubing (channel length = 2000 mm, I.D. = 1.0 mm) with various flow speeds (u, 1.0×10^{-4} – 1.0×10^{-2} m s^{-1}). The reaction mixture was poured into the methanol solution (15 mL) with a 5 M aqueous hydrochloric acid (HCl) solution (1.4×10^{-1} mL). The final products were centrifuged at 11,000 rpm for 30 min and washed three times with ethanol.

Synthesis of platinum nanosheets by gravity. Platinum nanosheets (PtNSs) were synthesized through a microreactor in the hyperswollen lyotropic lamellar (HL) phases. The heptane solution (21 mL) with $H_2PtCl_6 \cdot 6H_2O$ (1.0×10^{-1} wt%), Brij L4 (6.9 wt%), water (1.9 wt%), and methanol (8.7×10^{-1} wt%) and the heptane solution (21 mL) with $NaBH_4$ (2.6×10^{-2} wt%), Brij L4 (6.9 wt%), sodium hydroxide solution (pH 11) (1.9 wt%), and methanol (8.7×10^{-1} wt%) were separately poured into 25 mL syringes. The syringes were placed at various heights (h, 1150 – 2300 mm). The reaction mixture was poured into the methanol solution (15 mL) with a 5 M aqueous hydrochloric acid (HCl) solution (1.4×10^{-1} mL). The final products were centrifuged at 11,000 rpm for 30 min and washed three times with ethanol.

Synthesis of platinum fine particles. Platinum fine particles were synthesized in the heptane solution. The heptane solution (42 mL) with $H_2PtCl_6 \cdot 6H_2O$ (1.1×10^{-1} wt%), water (2.0 wt%), and methanol (9.3×10^{-1} wt%) was poured into a 100 mL beaker and stirred (300 rpm). The heptane solution (42 mL) with $NaBH_4$ (2.9×10^{-1} wt%), sodium hydroxide solution (pH11) (2.0 wt%), and methanol (9.3×10^{-1} wt%) was added to the 100 mL beaker. The final products were centrifuged at 11,000 rpm for 30 min and washed three times with ethanol.

RESULTS AND DISCUSSION

Stable HL phase with new compositions. The organic solutions of a commercially available surfactant Brij L4, a mixture containing tetraethyleneglycol monododecyl ether ($C_{12}E_4$) as the main

component, have been reported to exhibit HL phases with the addition of a small amount of water.[27] However, the HL phases are not stable without shear stress owing to the too low ratio of the hydrophilic part of Brij L4. We must stabilize the Brij L4 solution as a TRAP solution.[23] To search the appropriate additive for stabilizing the HL phase of the Brij L4 solution, we added commonly used alcohols as co-surfactants to the solution and checked if the solutions put between crossed nicols using a polarizing film wrapped around the vessel show the birefringence even without any shear stress, as shown in Figure 2a.[26] The polarized photograph of the heptane solution of Brij L4 and water does not show a texture typical of HL phases originating from their birefringence, as shown in Figure 2b. When we added methanol (0.41 wt%) to the heptane solution, this heptane solution exhibited birefringence, as shown in Figure 2c. The heptane solution also exhibited the Bragg reflection, as shown in Figure S1a. The reflection spectrum shown in Figure S1b indicates that the heptane solution has a one-dimensional periodic structure whose pitch is about 225 nm.[23] The heptane solution definitely forms an HL phase. The addition of methanol seems to enhance the stability of the HL phase by swelling the hydrophilic part of Brij L4. Methanol is likely placed at the interface as a co-surfactant like a surfactant and adjusts the volume ratio between the hydrophilic and hydrophobic parts of the surfactant. Ethanol and 1-propanol can also stabilize the HL phase, whereas 1-butanol and 1-pentanol cannot stabilize the HL phase, as shown in Figure S2. These results also indicate that the swelling of the hydrophilic part of the Brij L4 with these alcohols stabilizes the HL phase.

The increase of methanol does not destabilize the HL phase up to 1.55 wt%, as shown in Figure 2d. The heptane solution added methanol (1.92 wt%) does not exhibit the HL phase, as shown in Figure 2f. We defined a solution showing an HL phase only with stirring as a metastable state and an HL phase even without stirring as a stable state. This HL phase seems to be more stable than

the HL phase of its decane solution with methanol (0.41 wt%); this HL phase shows birefringence even without stirring.[26] The obtained phase diagram suggests that the HL phase exists only in a very small region, as shown in Figures 2g and S3.

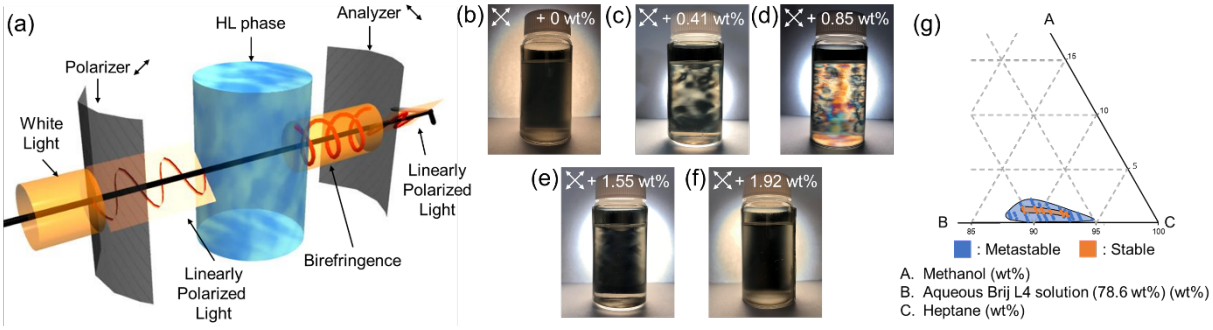

Figure 2. (a) The optical system to observe the birefringence of the heptane solution of Brij L4 with water using a polarizing film wrapped around a vessel while tilted at 45°. Polarized photographs of hyperswollen lyotropic lamellar phases of heptane solution of water (1.9 wt%) and Brij L4 (7.0 wt%). (b) No additives and (c) 0.41 wt%, (d) 0.85 wt%, (e) 1.55 wt% and (f) 1.92 wt% of methanol is added. (g) Triangular phase diagram of heptane, methanol, and an aqueous Brij L4 solution (78.6 wt%).

Stabilization of HL phase by plug flow. To synthesize PtNSs in a TRAP solution flowing through a microreactor, we should confirm whether the heptane solution of Brij L4 with water and methanol exhibits an HL phase there. We observed the flowing solution using the experimental setup shown in Figure S4. The heptane solution of Brij L4 with water and methanol was poured into the 25 ml syringe. The heptane solution was pumped into the polytetrafluoroethylene (PTFE) tubing with various flow speeds (u, 1.0×10^{-4} -1.0×10^{-2} m s^{-1}). The PTFE tubing was connected to a glass round capillary (I.D. = 1.05 mm) to observe the solution flowing through the capillary using a polarized optical microscope. The polarized photograph of the heptane solution at rest

shows birefringence, though it does not suggest the existence of any definite anisotropy, as shown in Figure 3a. Each of the polarized photographs of the heptane solution with the flow speed in the range from 1.0×10^{-4} to 1.0×10^{-2} m s^{-1} shows a black horizontal line at the center of the glass capillary, and the black line becomes clearer as the flow speed increases, as shown in Figures 3b-3d. These results imply that the TRAPs were arranged parallel to the direction of the flow, as shown in Figure 3e.

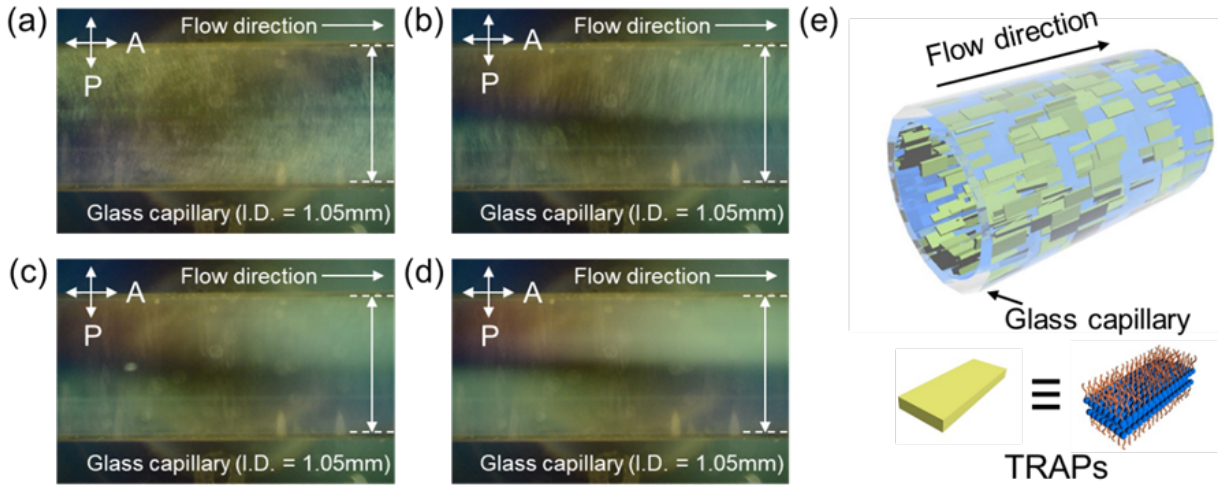

Figure 3. The liquid crystalline texture of hyperswollen lyotropic lamellar phases of heptane solution of water (1.9 wt%), Brij L4 (6.9 wt%) and methanol (8.7×10^{-1} wt%) inside a glass round capillary. The average flow rate is (a) 0, (b) 1.0×10^{-4} m s^{-1}, (c) 1.0×10^{-3} m s^{-1}, and (d) 1.0×10^{-2} m s^{-1}. (e) Schematic illustration of the orientation of TRAPs along the flow direction.

Synthesis of PtNSs by using syringe pumps. The HL phases of the TRAP solutions have to be stable even in the presence of the ingredients of PtNSs. Therefore, we observed the TRAP solutions dissolving hydrogen hexachloroplatinate (IV) hexahydrate ($H_2PtCl_6 \cdot 6H_2O$) and sodium borohydride ($NaBH_4$) separately and found that the HL phases are still stable, as shown in Figures

4a and 4b. The hydrophilic bilayers are likely to trap H_2PtCl_6 and $NaBH_4$ stably. Then, we tried to synthesize PtNSs through a microreactor using a syringe pump, as shown in Figure S5. A TRAP solution dissolving H_2PtCl_6 and another TRAP solution dissolving $NaBH_4$ were separately poured through PTFE tubing into a mixer. The mixture was pumped into a reaction tubing (channel length = 2000 mm, I.D. = 1.0 mm) with various flow speeds (u, 1.0×10^{-4} – 1.0×10^{-2} m s^{-1}). We employ the constant concentration of the precursor because the averaged width and thickness of NSs synthesized by the TRAP method are independent of the concentration of the precursor.[26]

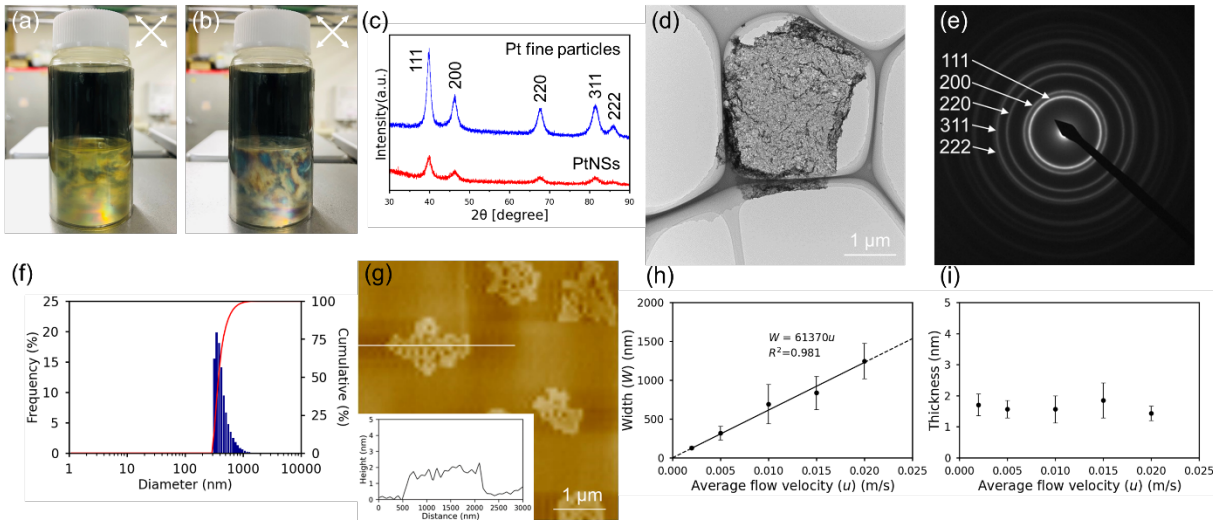

Figure 4. Reaction conditions and characterization of obtained PtNSs. Polarized photographs of hyperswollen lyotropic lamellar phases of (a) heptane solution of water (1.9 wt%), Brij L4 (6.9 wt%), methanol (8.7×10^{-1} wt%), and H_2PtCl_6 (8.3×10^{-2} wt%), and (b) heptane solution of water (1.9 wt%), Brij L4 (6.9 wt%), methanol (8.7×10^{-1} wt%), and $NaBH_4$ (2.7×10^{-2} wt%). (c) X-ray diffraction patterns of the PtNSs, and Pt fine particles. (d) TEM photograph of PtNSs, and (e) SAED pattern of PtNSs. (f) DLS analysis of PtNSs. (g) AFM photograph and cross-section of one of the synthesized PtNSs. Dependence of the PtNSs size on u. (h) width and (i) thickness of the PtNSs.

The reaction mixture collected from a microreactor (u = 1.0 × 10^{-2} m s^{-1}) was centrifuged at 11,000 rpm for one hour, and the precipitate was washed three times with methanol to give a black powder (25 % yield). The X-ray diffraction (XRD) pattern of the black powder showed the same peaks and intensity ratios as Pt fine particles, which were synthesized in the heptane solution without Brij L4 at the 100 ml beaker, as shown in Figures 4c and S6. The obtained black powder seems to be crystalline metallic Pt^0, and the growth inhibition of some certain crystal planes does not occur. The transmission electron microscopy (TEM) photographs indicate that the samples are sheet-like particles, as shown in Figures 4d and S7. The selected area electron diffraction (SAED) pattern provides evidence of the crystallinity of the sample, as shown in Figures 4e and S7. The SAED pattern also indicates that PtNSs are polycrystals of small crystals; it shows concentric circles. The particle size distributions estimated from dynamic light scattering (DLS) measurements of the products look sharp, as shown in Figure 4f. All the products are likely to be monodispersed. The horizontal width and thickness of the products measured by atomic force microscopy (AFM) are 1247 ± 228 and 1.44 ± 0.23 nm, respectively, as shown in Figures 4g and S8. In contrast, the sample synthesized without microfluidic devices was PtNSs, as shown in Figure S9. These results indicate that the TRAPs, not microfluidic devices, promote the lateral growth of PtNSs. The uniformly nanosized Pt particles look laterally fused nanoplatelets in the confined thin 2-D reaction field of the HL phase. These results indicate that the products are thin crystalline metallic PtNSs.[5]

The thermogravimetric analysis of PtNSs did not detect weight reduction between 200 °C and 400 °C, where Brij L4 shows weight reduction, as shown in Figure S10. The amphiphile Brij L4 should not protect the surface of the PtNSs. Besides, the full width at half maximum (FWHM) of each of the XRD peaks for the obtained powder was broader than that of the isotropically grown

Pt fine particles with a diameter of several hundred nm, as shown in Table S1. The Williamson-Hall plots shown in Figure S11 indicate that the crystallite size of the obtained powder is smaller than that of Pt fine particles.[36] The physically confined Pt nanoplatelets should be bonded to give NSs. The surface of the PtNSs could be stable, unlike the previously reported single-crystalline PtNSs.[37]

We measured the *u*-dependence of the obtained particle size, as shown in Table S2. The width and thickness of the PtNSs for each of several synthetic conditions were measured using AFM, as shown in Figure S12, and the size distribution of these PtNSs was estimated from DLS measurements, as shown in Figure S13. The width of PtNSs seems to be proportional to *u*, as shown in Figure 4h. Meanwhile, the thickness is probably independent of *u*, as shown in Figure 4i. We have successfully confirmed that local anisotropy can be mechanochemically controlled using flow speed as a global process variable. Besides, the particle width is also proportional to the Reynolds number, the ratio of inertial force to viscous force, as listed in Table S2. It suggests that the bilayer area in the HL phase proportional to shear stress increases the particle width.[22,26] This mechanochemical synthesis of NSs is probably easy to apply to various materials because the Reynolds number is controlled using the dynamic viscosity of the reaction mixture and cross-sectional area of the flow reactor. Syringe pumps electrically generate the mechanical energy to accelerate the lateral fusion of the Pt nanoplatelets and control the width of the PtNSs. Mechanical energy can be extracted in various ways.

Synthesis of PtNSs by gravity. Gravity is the most universal and eco-friendly energy source on the earth. We tried to control the lateral growth of PtNSs using gravity, as shown in Figure S14. A TRAP solution dissolving H_2PtCl_6 and another TRAP solution dissolving $NaBH_4$ were separately poured into the 25 ml syringe. The syringes were placed at the height of 2300 mm. The

particle size distributions estimated from DLS of the aqueous dispersion of the products suggest the absence of the aggregates, as shown in Figure S15a. The thickness and horizontal width of the products measured by AFM are 2.6 ± 0.87 nm and 557 ± 112 nm, respectively, as shown in Figure S15b. We measured the dependence of the particle size on the height of the syringe (h), as shown in Figures S16 and S17 and Table S3. First, we confirmed the h-dependence of u, as shown in Figure S18. We can fit the h-dependence of u with

$$u = \sqrt{19.6h + \left(\frac{32I\mu}{d^2}\right)^2} - \left(\frac{32I\mu}{d^2}\right) + \sqrt{\frac{f}{\rho}}, \quad (1)$$

where I is the length of the flow channel, μ is viscosity, d is the inner diameter of the flow channel, f is the free energy density of TRAP solution, and ρ is the density of the solution, as shown in Figure S19 (see Supporting Information). We could decide the h-dependence of the width of PtNSs, as shown in Figure S16f. However, we could not achieve the quantitative correlation between the syringe pump method and the gravity-based method because of the difficulty of matching the flow rates of the ingredient solutions in the gravity-based method. Besides, the thickness seems independent of h, as shown in Figure S16g. The thickness of the PtNSs obtained at the height of 2300 mm is thicker than the others. The PtNSs probably grow thicker when the reaction time in the microreactor is too short because the unreacted ingredients cause the nanosheets to grow isotropically. We can conclude that it is possible to control the aspect ratio of PtNSs by transforming gravitational potential energy to local mechanical stress.

Catalytic reaction test. We examined the dispersity of the synthesized PtNSs in various solvents without Brij L4, as shown in Figure S20: hexane, diethyl ether, ethyl acetate, toluene, chloroform, tetrahydrofuran, and acetone. The PtNSs were well dispersed in the toluene, chloroform, THF, and acetone. In contrast, they were not well dispersed in hexane, diethyl acetate

and ethyl acetate to precipitate, as shown in Figure S21. In contrast, the Pt fine particles were not dispersed, as shown in Figure S22. The precipitates generated in hexane can be redispersed in ethanol again, as shown in Figures S23 and S24. This result indicates that the precipitation in hexane was caused by the hydrophilicity of PtNSs, not the surface free energy. We guess that nanoparticles with various orientations constituting the PtNSs allow the coexistence of aggregation inhibition and higher reactivity.

We examined the catalytic activity of the obtained PtNSs for the reduction reaction of 4-nitrophenol (4-NP) to 4-aminophenol (4-AP), as shown in Figure S25.[38] This reaction can be easily monitored using UV-visible spectroscopy because nitrophenolate ions and 4-AP display absorption bands centered at 400 nm and 300 nm, respectively. After adding the PtNSs into the 4-NP solution, the intensity of the absorption peaks at 400 nm gradually decreased, and the intensity of the new peak for 4-AP at 317 nm increased, as shown in Figure 5a. Since we used an excessive amount of the reductant $NaBH_4$, the reaction can be assumed to be independent of $NaBH_4$ concentration and expected to follow pseudo-first-order kinetics,

$$-\frac{\mathrm{d}[\text{4-NP}]}{\mathrm{d}t} = k_{\mathrm{app}}[\text{4-NP}] \tag{2}$$

$$\ln\frac{[\text{4-NP}]}{[\text{4-NP}]_0} = -k_{\mathrm{app}} \cdot t, \tag{3}$$

where [4-NP] and $[4\text{-NP}]_0$ are the concentrations of 4-nitrophenolate at time t and 0, respectively, and

$$\ln([\text{4-NP}]/[\text{4-NP}]_0) = \ln(A/A_0), \tag{4}$$

where A and A_0 are the corresponding absorbances of the typical band at 400 nm, respectively. We fitted a plot of $\ln(A/A_0)$ vs. reaction time to a first-order rate equation, as shown in Figure 5b, and

calculated the rate constant as 0.23 min^{-1}. To compare our results with previously reported ones, we determined the normalized rate constant (k_{nor}) by

$$k_{nor} = k_{app}/(m[NaBH_4]) \quad (5)$$

where k_{app} is normalized about the total amount of the catalyst (m) and the borohydride concentration ([$NaBH_4$]). The k_{nor} value obtained for the PtNSs was 3886 g^{-1} s^{-1} M^{-1}. This value is greater than the k_{nor} estimated for other catalysts, as shown in Table S4. This result should come from the increase of the relative surface area.

The catalytic activity of PtNSs increases with the width of PtNSs, as shown in Figures 5c and S26. Size distribution after the reaction shown in Figure S27 indicates that the small PtNSs agglomerated. The formation process of the PtNSs is probably important to explain the surprising results. The PtNSs grow with the anisotropic fusion of nanoplatelets in TRAPs, as shown in Figures 1c, 4d and 4g. These crystallites have random orientation, as indicated by the XRD profiles shown in Figure 4c. Generally speaking, the aggregation of two Pt nanoparticles occurs when the active surfaces are attached, and they lose their catalytic activity.[39] We consider the following mechanism. The PtNSs grown in TRAPs has some active sites. The aggregation of two small PtNSs occurs when the patterns of the active surfaces are matched, and they are attached and lose their catalytic activity. The wider the PtNSs are, the less often the aggregation occurs. The more various the patterns of the active sites are, the more inconsistent the patterns are, as shown in Figure 5d.

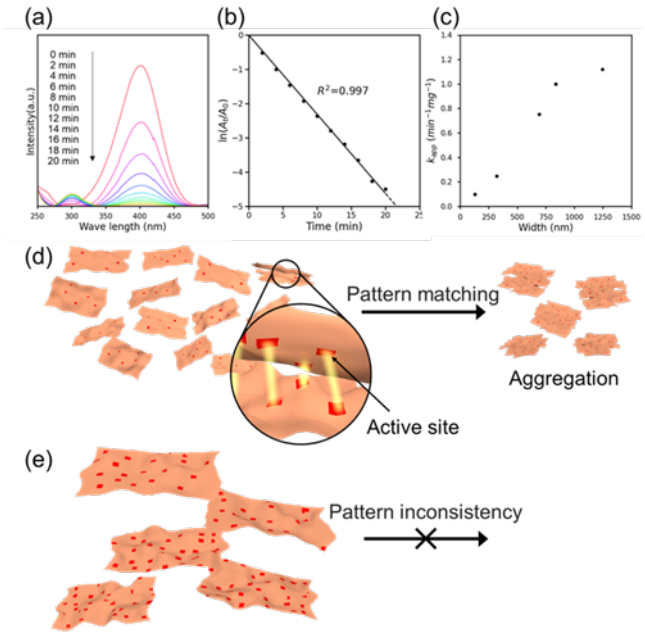

Figure 5. (a) Successive UV–Vis spectra of the reduction of 4-NP in the presence of NaBH4 using PtNSs as catalysts. (b) The relationship between $\ln(C_t/C_0)$ and reaction time, in which the ratio of 4-nitrophenol (C_t at time t) to its initial value C_0 was directly obtained by the relative intensity of the respective absorbance A_t/A_0 with absorption peaks at 400 nm. (c) The dependence of k_{app} of PtNSs on the width of PtNSs. Schematic illustration of the stacking of PtNSs. (d) Active sites are attached for the small PtNSs, whereas (e) active sites at the random configuration in the larger PtNSs prevent the aggregation.

CONCLUSIONS

In summary, several nm thick dispersible PtNSs have been successfully synthesized in a TRAP solution through a microreactor. It is the first example of the fabrication of non-layered compounds by the bottom-up synthesis in a microreactor. The stability of the TRAP solution was dramatically enhanced by only adding the methanol due to the swelling of the hydrophobic part of the Brij L4. The newly found composition showing an HL phase enables us to reuse the solvent and synthesize

high-quality nanosheets in larger quantities and at lower costs. The TRAP solution can emerge an HL phase in a glass round capillary, and the TRAPs were arranged parallel to the direction of the flow. The PtNSs' width seems to be proportional to the Reynolds number of the system because the bilayer area in the HL phase depends on shear stress. The width of the TRAPs depends on the shear stress. We also confirmed that we could control the PtNSs' width using gravity. It is also the first example of the fabrication of anisotropic nanoparticles by using gravity. Because of the high dispersibility attributed to the lateral fusion of nanoplatelets, the PtNSs show higher catalytic activity for the reduction reaction of 4-nitrophenol to 4-aminophenol than the other metal nanoparticles. This study is the first example of finding a size dependence of catalytic activity. The PtNSs perform better in catalysis and should work well in hydrogen production, fuel cells, and sensors because of their large surface area and dispersibility. This method can apply to NSs of other metals,[26] metal oxides, organometallic complexes,[24,25,27] polymers,[23] and organic crystals.

ASSOCIATED CONTENT

The Supporting Information is available free of charge on the ACS Publications website.

Synthesis method, characterization methods, triangular phase diagram, scheme and photograph of experimental setup, TEM photograph, electron diffraction pattern, TG analysis curve, XRD peak position and FWHM, Williamson-Hall plots, photographs of suspensions of PtNSs with various solvents, size distributions, AFM photographs, and comparison of catalytic activity (PDF)

AUTHOR INFORMATION

Corresponding Author

*Yoshiaki Uchida – Graduate School of Engineering Science, Osaka University, Toyonaka, Osaka 560-8531, Japan; orcid.org/0000-0001-5043-9239;

Email: y.uchida.es@osaka-u.ac.jp

Notes

The authors declare no competing financial interest.

ACKNOWLEDGMENT

The authors thank Prof. T. Hirai and Prof. Y. Shiraishi for their help with the use of dynamic light scattering photometer. This work was supported in part by the Advanced Characterization Nanotechnology Platform, Nanotechnology Platform Program of the Ministry of Education, Culture, Sports, Science and Technology (MEXT), Japan, Grant Number JPMXP09A21OS0028 at the Research Center for Ultra-High Voltage Electron Microscopy (Nanotechnology Open Facilities) in Osaka University, and JSPS KAKENHI Grant Number JP20H05161.

REFERENCES

(1) Murphy, C. J.; Sau, T. K.; Gole, A.; Orendorff, C. J. Surfactant-Directed Synthesis and Optical Properties of One-Dimensional Plasmonic Metallic Nanostructures. *MRS Bull*. **2005**, *30*, 349–355.

(2) Shirale, D. J.; Bangar, M. A.; Chen, W.; Myung, N. V.; Mulchandani, A. Effect of Aspect Ratio (Length:Diameter) on a Single Polypyrrole Nanowire FET Device. *J. Phys. Chem. C* **2010**, *114*, 13375–13380.

(3) Ferk, G.; Krajnc, P.; Hamler, A.; Mertelj, A.; Cebollada, F.; Drofenik, M.; Lisjak, D. Monolithic Magneto-Optical Nanocomposites of Barium Hexaferrite Platelets in PMMA. *Sci. Rep.* **2015**, *5*, 11395.

(4) Jiji, S. G.; Gopchandran, K. G. Shape dependent catalytic activity of unsupported gold nanostructures for the fast reduction of 4-nitroaniline. *Colloid Interface Sci. Commun.* **2019**, *29*, 9–16.

(5) Funatsu, A.; Tateishi, H.; Hatakeyama, K.; Fukunaga, Y.; Taniguchi, T.; Koinuma, M.; Matsuura, H.; Matsumoto, Y. Synthesis of monolayer platinum nanosheets. *Chem. Commun.* **2014**, *50*, 8503–8506.

(6) Ye, S.; Azad, A. A.; Chambers, J. E.; Beckett, A. J.; Roach, L.; Moorcroft, S. C. T.; Aslam, Z.; Prior, I. A.; Markham, A. F.; Coletta, P. L.; Marciniak, S. J.; Evans, S. D. Exploring High Aspect Ratio Gold Nanotubes as Cytosolic Agents: Structural Engineering and Uptake into Mesothelioma Cells. *Small* **2020**, *16*, 2003793.

(7) Murphy, C. J.; Jana, N. R. Controlling the Aspect Ratio of Inorganic Nanorods and Nanowires. *Adv. Mater.* **2002**, *14*, 80–82.

(8) Zhu, D.; Zhu, H.; Zhang, Y. H. Hydrothermal synthesis of single-crystal $La_{0.5}Sr_{0.5}MnO_3$ nanowire under mild conditions. *J. Phys.: Condens. Matter* **2002**, *14*, L519–L524.

(9) Yang, Q.; Sha, J.; Ma, X.; Yang, D. Synthesis of NiO nanowires by a sol-gel process. *Mater. Lett.* **2005**, *59*, 1967–1970.

(10) Liu, Y.; Cao, J.; Zeng, J.; Li, C.; Qian, Y.; Zhang, S. A Complex-Based Soft Template Route to PbSe Nanowires. *Eur. J. Inorg. Chem.* **2003**, 644–647.

(11) Dai, H.; Wong, E. W.; Lu, Y. Z.; Fan, S.; Lieber, C. M. Synthesis and characterization of carbide nanorods. *Nature* **1995**, *375*, 769–772.

(12) MacEwan, D. M. C.; Wilson, M. J. in *Crystal Structures of Clay Minerals and Their X-ray Identification*; Brindley, G. W.; Brown, G. Eds.; Mineralogical Society of Great Britain and Ireland: Middlesex, United Kingdom, **1980**, Chapter 3, p 197.

(13) Iijima, S. Helical microtubules of graphitic carbon. *Nature* **1991**, *354*, 56–58.

(14) Tanaka, S., Nishiyama, N., Egashira, Y., Ueyama, K. Synthesis of ordered mesoporous carbons with channel structure from an organic–organic nanocomposite. *Chem. Commun.*, **2005**, *16*, 2125–2127.

(15) Ota, M.; Hirota, Y.; Uchida, Y.; Sakamoto, Y.; Nishiyama, N. Low Temperature Synthesized $H_2Ti_3O_7$ Nanotubes with a High CO_2 Adsorption Property by Amine Modification. *Langmuir* **2018**, *34*, 6814–6819.

(16) Kang, S. K.; Kim, Y.; Hahn, M. S.; Choi, I.; Lee, J.; Yi, J. Aspect ratio control of Au nanorods via temperature and hydroxylamine concentration of reaction medium. *Curr. Appl Phys.* **2006**, *6*, e114–e120.

(17) Jeevanandam, J.; Barhoum, A.; Chan, Y. S.; Dufresne, A.; Danquah, M. K. Review on nanoparticles and nanostructured materials: history, sources, toxicity and regulations. *Beilstein J. Nanotechnol.* **2018**, *9*, 1050–1074.

(18) Yao, Y. G.; Lin, Z.; Li, Z.; Song, X. J.; Moon, K. S.; Wong, C. P. Large-scale production of two-dimensional nanosheets. *J. Mater. Chem.* **2012**, *22*, 13494–13499.

(19) Lehmann, O. Structur, System und magnetisches Verhalten flüssiger Krystalle und deren Mischbarkeit mit festen. *Ann. Phys.* **1900**, *4*, 649–705.

(20) Kahn, F. J. Electric-Field-Induced Color Changes and Pitch Dilation Cholesteric Liquid Crystals. *Phys. Rev. Lett.* **1970**, *24*, 209–212.

(21) Safinya, C. R.; Sirota, E. B.; Plano, R. J. Nematic to Smectic-A Phase Transition Under Shear Flow: A Nonequilibrium Synchrotron X-Ray Study. *Phys. Rev. Lett.* **1991**, *66*, 1986–1989.

(22) Yamamoto, J.; Tanaka, H. Shear Effects on Layer Undulation Fluctuations of a Hyperswollen Lamellar Phase. *Phys. Rev. Lett.* **1995**, *74*, 932–935.

(23) Uchida, Y.; Nishizawa, T.; Omiya, T.; Hirota, Y.; Nishiyama, N. Nanosheet Formation in Hyperswollen Lyotropic Lamellar Phases. *J. Am. Chem. Soc.* **2016**, *138*, 1103–1105.

(24) Omiya, T.; Sasaki, K.; Uchida, Y.; Nishiyama, N. Nanosheet Synthesis of Metal Organic Frameworks in a Sandwich-like Reaction Field for Enhanced Gate-Opening Pressures. *ACS Appl. Nano Mater.* **2018**, *1*, 3779–3784.

(25) Omiya, T.; Sasaki, K.; Uchida, Y.; Nishiyama, N. Synthesis of MOF Nanosheets in Hyperswollen Lyotropic Lamellar Phase. *Mol. Cryst. Liq. Cryst.* **2019**, *684*, 1–6.

(26) Sasaki, K.; Okue, T.; Nakai, T.; Uchida, Y.; Nishiyama, N. Lateral Growth of Uniformly Thin Gold Nanosheets Facilitated by Two-Dimensional Precursor Supply. *Langmuir* **2021**, *37*, 5872–5877.

(27) Sasaki, K.; Okue, T.; Shu, Y.; Miyake, K.; Uchida, Y.; Nishiyama, N. Thin ZIF-8 Nanosheets Synthesized in Hydrophilic TRAPs. *Dalton Trans.*, **2021**, *50*, 10394–10399.

(28) Larche, F. C.; Appell, J.; Porte, G.; Bassereau, P.; Marignan, J. Extreme Swelling of a Lyotropic Lamellar Liquid Crystal. *Phys. Rev. Lett.* **1986**, *56*, 1700–1703.

(29) Kubota, K.; Pang, Y.; Miura, A.; Ito, H. Redox reactions of small organic molecules using ball milling and piezoelectric materials. *Science*. **2019**, *366*, 1500–1504.

(30) Elvira, K. S.; i Solvas, X. C.; Wootton, R. C. R.; deMello, A. J. The past, present and potential for microfluidic reactor technology in chemical synthesis. *Nat. Chem.* **2013**, *5*, 905–915.

(31) Amreen, K.; Goel, S. Review—Miniaturized and Microfluidic Devices for Automated Nanoparticle Synthesis. *ECS J. Solid State Sci. Technol.* **2021**, *10*, 017002.

(32) Choi, C.-H.; Kwak, Y.; Malhotra, R.; Chang, C.-H. Microfluidics for Two-Dimensional Nanosheets: A Mini Review. *Processes* **2020**, *8*, 1067.

(33) Wang, Y.; Li, L.; Yan, L.; Gu, X.; Dai, P.; Liu, D.; Bell, J. G.; Zhao, G.; Zhao, X.; Thomas, K. M. Bottom-Up Fabrication of Ultrathin 2D Zr Metal–Organic Framework Nanosheets through a Facile Continuous Microdroplet Flow Reaction. *Chem. Mater.* **2018**, *30*, 3048–3059.

(34) Xu, W.; Zheng, H.; Liu, Y.; Zhou, X.; Zhang, C.; Song, Y.; Deng, X.; Leung, M.; Yang, Z.; Xu, R. X.; Wang, Z. L.; Zeng, X. C.; Wang, Z. A Droplet-Based Electricity Generator with High Instantaneous Power Density. *Nature* **2020**, *578*, 392–396.

(35) Mourdikoudis, S.; Altantzis, T.; Liz-Marzan, L. M.; Bals, S.; Pastoriza-Santos, I.; Perez-Juste, J. Hydrophilic Pt nanoflowers: synthesis, crystallographic analysis and catalytic performance. *CrystEngComm* **2016**, *18*, 3422–3427.

(36) Williamson, G. K.; Hall, W. H. X-ray line broadening from filed aluminium and wolfram. *Acta Metall*. **1953**, *1*, 22–31.

(37) Takenaka, S.; Arita, H.; Sugiyama, K.; Nakatani, K. Preparation of Pt Nanosheets Using Graphene Oxide. *Chem. Lett*. **2018**, *47*, 975–978.

(38) Alegria, E. C. B. A.; Ribeiro, A. P. C.; Mendes, M.; Ferraria, A. M.; do Rego, A. M. B.; Pombeiro, A. J. L. Effect of Phenolic Compounds on the Synthesis of Gold Nanoparticles and Its Catalytic Activity in the Reduction of Nitro Compounds. *Nanomaterials* **2018**, *8*, 320.

(39) Ma, Y.; Gao, W.; Shan, H.; Chen, W.; Shang, W.; Tao, P.; Song, C.; Addiego, C.; Deng, T.; Pan, X.; Wu, J. Platinum-Based Nanowires as Active Catalysts toward Oxygen Reduction Reaction: In Situ Observation of Surface-Diffusion-Assisted, Solid-State Oriented Attachment. *Adv. Mater*. **2017**, *29*, 1703460.

TOC graphic

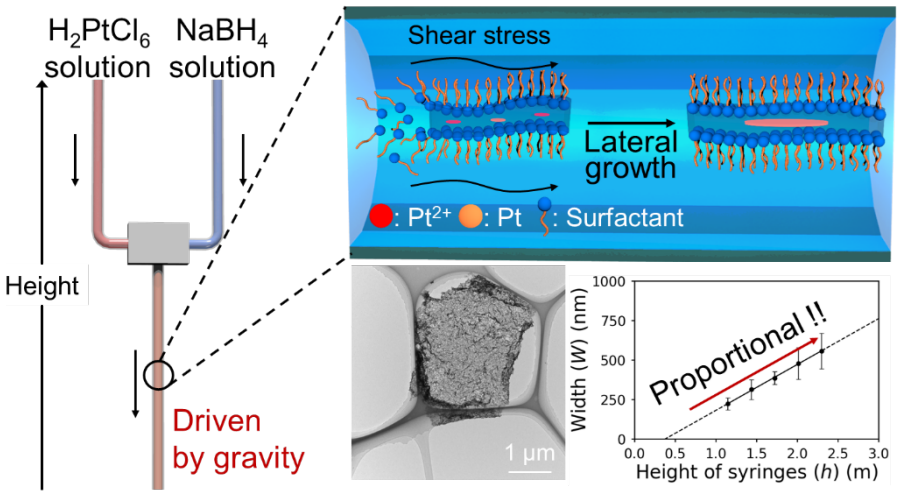
H_2PtCl_6 solution
$NaBH_4$ solution
Height
Driven by gravity
Shear stress
Lateral growth
: Pt^{2+}
: Pt
: Surfactant
1 μm
Width (W) (nm)
1000
750
500
250
0
0.0
0.5
1.0
1.5
2.0
2.5
3.0
Height of syringes (h) (m)
Proportional !!